Applied Physics Research; Vol. 4, No. 3; 2012
ISSN 1916-9639 E-ISSN 1916-9647
Published by Canadian Center of Science and Education

Structure and Stability of BCC Crystals Fe, V, Nb and Ta under Hydrostatic Loading

Jingzhou Wang[1] & Yongjie Dai[1]

[1] Ordos College of Inner Mongolia University, Ordos, China

Correspondence: Jingzhou Wang, Ordos College of Inner Mongolia University, Ordos 017000, China. E-mail: wangjingzhou1101@126.com

Received: March 18, 2012 Accepted: April 6, 2012 Online Published: July 15, 2012

doi:10.5539/apr.v4n3p8 URL: http://dx.doi.org/10.5539/apr.v4n3p8

Abstract

The structural stability and theoretical strength of BCC crystals Fe, V, Nb and Ta under hydrostatic loading have been investigated by using the modified analytical embedded atom method (MAEAM). For all the calculated BCC crystals, the failures occur while the relation $\mu>0$ is violated in compression and $\kappa>0$ is violated in tension. It found that the stable regions are 0.9269~1.1495, 0.9270~1.1545, 0.9268~1.1449 and 0.9268 ~ 1.1427 in the lattice stretch λ or the corresponding -408.89 ~ 123.54, -186.96 ~ 131.43, -259.07 ~ 152.53 and -283.92 ~137.04eV/nm^3 in the theoretical strength for Fe, V, Nb and Ta, respectively. The calculated maximum tensile stresses σ_{max} of Fe, V, Nb and Ta are 123.57, 131.74, 154.45 and 137.85eV/nm^3 and the corresponding lattice stretch $\lambda_{max.}$ are 1.1527, 1.1617, 1.1661 and 1.1545. The calculated maximum tensile stress σ_{max} and the corresponding lattice stretch λ_{max} of Fe are consistent well with the results of Ab initio calculation.

Keywords: Fe crystal, stability, theoretical strength, MAEAM

1. Introduction

Triaxial tension occurs in solids in the vicinity of some types of defects in the microstructure of crystalline solids, e.g., cracks, pores, voids, and complex phase or grain boundaries (Kelly & Macmillan, 1986). To understand the structure and behavior of these defects, information on local elastic constants and theoretical (ideal) strength is necessary. For example, the theoretical strength of a perfect crystal plays an important role in determining the stress distribution near the tip of a crack and is important in determining whether a material will exhibit brittle or ductile behavior (Kelly, 1966).

The theoretical strength of a material is defined as the stress at which a homogeneously deformed perfect crystal becomes elastically unstable with respect to internal displacements (Clatterbuck, Chrzan, & Morris Jr, 2003). The stable region is sensitive to the behavior of the loading mechanism and the theoretical strength is strongly depends on the direction of tension or compression since it is anisotropic. For these interesting properties, the structural and theoretical strength of solids have been widely investigated with many experimental (Fuente et al., 2002) and theoretical (Kanchana, Vaitheeswaran, & Rajagopalan, 2003) methods. Experimentally, the whiskers or nanoindentation experiments were used to investigate the stability or theoretical strength of the crystals under pressure. Theoretically, many simulation methods, such as the linear muffin-tin orbital (LMTO) method, the pair-potential theory (Milstein & Huang, 1978), the embedded-atom method (EAM) (Milstein and Chantasiriwan, 1998), the molecular-dynamics (MD) simulation (Qi, Zhang, & Hu, 2004), Ab initio calculation (Saib & Bouarissa, 2007) etc., have been used. Among all the theoretical methods, the Ab initio calculation based on quantum mechanics is thought to be the most precise, however, the complex calculations and long computation time requires higher-performance computing.

Some properties of body-centered cubic (BCC) crystal Fe under hydrostatic loading (Černý et al., 2003) have been investigated with Ab initio. The main purpose of this paper is to compute theoretical strength and find out the stable region of BCC crystal Fe, V, Nb, and Ta under hydrostatic loading by using the modified analytical embedded atom method (MAEAM). This method has been used successfully in our previous papers to analyze the stability of the face-centered cubic (FCC) crystal Ni (Zhang, Li, & Xu, 2007), Au (Zhang et al., 2008a) and the BCC crystal Fe (Zhang et al., 2008b) under uniaxial loading and BCC transition metals Cr, Mo and W (Li, Zhang, & Xu, 2008) under hydrostatic loading respectively and the other properties of the metals and alloys.

2. Simulation Method

2.1 MAEAM

In MAEAM, the total energy of a system E_t is expressed as

$$E_t = \sum_i E_i = \sum_i \left[F(\rho_i) + \frac{1}{2} \sum_{j(\neq i)} \phi(r_{ij}) + M(P_i) \right] \tag{1}$$

in which

$$\rho_i = \sum_{j(\neq i)} f(r_{ij}) \tag{2}$$

$$P_i = \sum_{j(\neq i)} f^2(r_{ij}) \tag{3}$$

where E_i is the energy contribution from atom i to the total energy E_t, $F(\rho_i)$ is the energy to embed an atom in site i with electron density ρ_i which is given by a linear superposition of the spherical averaged atomic electron densities of other atoms $f(r_{ij})$, r_{ij} is the separation distance of atom j from atom i, $\phi(r_{ij})$ is the pair potential between atoms i and j, and $M(P_i)$ is the modified term which describes the energy change due to the deviation from the linear superposition. The embedding function $F(\rho_i)$, pair potential $\phi(r_{ij})$, modified term $M(P_i)$ and atomic electron density $f(r_{ij})$ take the following forms

$$F(\rho_i) = -F_0 \left[1 - \ln\left(\frac{\rho_i}{\rho_e} \right) \right] \left(\frac{\rho_i}{\rho_e} \right)^n \tag{4}$$

$$\phi(r_{ij}) = k_0 + k_1 \left(\frac{r_{ij}}{r_{1e}} \right)^2 + k_2 \left(\frac{r_{ij}}{r_{1e}} \right)^4 + k_3 \left(\frac{r_{1e}}{r_{ij}} \right)^{12} \qquad \left(r_{ij} \le r_{2e} \right) \tag{5}$$

$$M(P_i) = \alpha \left(\frac{P_i}{P_e} - 1 \right)^2 \exp\left[-\left(\frac{P_i}{P_e} - 1 \right)^2 \right] \tag{6}$$

$$f(r_{ij}) = f_e \left(\frac{r_{1e}}{r_{ij}} \right)^6 \tag{7}$$

where the subscript e indicates equilibrium state and r_{1e} is the first nearest neighbor distance at equilibrium. In this paper, the atomic election density at equilibrium f_e is chosen as

$$f_e = \left(\frac{E_c - E_{1f}}{\Omega} \right)^{3/5} \tag{8}$$

where $\Omega = \frac{a_0^3}{2}$ is the atomic volume in BCC metals (a_0 is the unstressed lattice constant), E_c and E_{1f} are cohesion energy and mono-vacancy formation energy, respectively.

The other parameters n, F_0, α, k_0, k_1, k_2 and k_3 in Eqs. (4)-(6) can be determined by cohesion energy E_c, mono-vacancy formation energy E_{1f}, lattice constant a_0, and elastic constants C_{11}, C_{12}, C_{44} of the metals considered

$$n = \sqrt{\frac{\Omega(C_{11} + 2C_{12})(C_{11} - C_{12})}{216 E_{1f} C_{44}}} \tag{9}$$

$$F_0 = E_c - E_{1f} \tag{10}$$

$$\alpha = \frac{\Omega\left(C_{12} - C_{44}\right)}{32} - \frac{n^2 F_0}{8} \tag{11}$$

$$k_0 = -\frac{E_{1f}}{7} - \frac{\Omega\left(51519C_{44} + 57111C_{12} - 57111C_{11}\right)}{471800} \tag{12}$$

$$k_1 = \frac{\Omega\left(33327C_{44} + 52563C_{12} - 52563C_{11}\right)}{269600} \tag{13}$$

$$k_2 = \frac{\Omega\left(147456C_{11} - 147456C_{12} - 59049C_{44}\right)}{1887200} \tag{14}$$

$$k_3 = \frac{1536\Omega\left(4C_{44} - C_{11} + C_{12}\right)}{412825} \tag{15}$$

According analysis of Zhang et al, the pair-potential $\phi(r_{ij})$ represented by Eq. (5) can be used only for the separated distance between atoms is shorter than the second neighbor distance r_{2e} and should be substituted by following cubic spline function (termed as a cutoff potential) while the separated distance between atoms ranges from r_{2e} to r_c.

$$\phi(r_{ij}) = l_0 + l_1\left(\frac{r_{ij}}{r_{2e}} - 1\right) + l_2\left(\frac{r_{ij}}{r_{2e}} - 1\right)^2 + l_3\left(\frac{r_{2e}}{r_{ij}} - 1\right)^3 \qquad \left(r_{2e} < r_{ij} \le r_c\right) \tag{16}$$

Four parameters l_0, l_1, l_2, l_3, and cutoff radius r_c are taken as

$$l_0 = k_0 + k_1 s^2 + k_2 s^4 + k_3 s^{-12} \tag{17}$$

$$l_1 = 2k_1 s^2 + 4k_2 s^4 - 12k_3 s^{-12} \tag{18}$$

$$l_2 = -\frac{2l_1}{\gamma - 1} - \frac{3l_0}{(\gamma - 1)^2} \tag{19}$$

$$l_3 = \frac{l_1}{(\gamma - 1)^2} + \frac{2l_0}{(\gamma - 1)^3} \tag{20}$$

$$r_c = r_{2e} + 0.75\left(r_{3e} - r_{2e}\right) \tag{21}$$

where r_{2e} and r_{3e} are the second and the third neighbor distance at equilibrium, and $s = \frac{r_{2e}}{r_{1e}}$, $\gamma = \frac{r_c}{r_{2e}}$.

By substituting physical parameter a_0, E_c, E_{1f}, C_{11}, C_{12} and C_{44} (listed in Table 1) into Eqs. (8)-(15), we can obtained the model parameters for Fe, V, Nb, and Ta (see Table 2).

Table 1. The input physical parameters for Fe, V, Nb and Ta, a_0 is in nm, E_c and E_{1f} in eV and C_{ij} in GPa.

Metals	a_0	E_c	E_{1f}	C_{11}	C_{12}	C_{44}
Fe	0.28664	4.28	1.79	230	135	117
V	0.30282	5.31	2.10	230	120	43.2
Nb	0.33007	7.57	2.75	245	132	28.4
Ta	0.33026	8.10	2.95	262	156	82.6

2.2 The Stability Criteria

For a cubic crystal undergoing homogeneous deformation, the strains ε_α of the crystal are expressed as:

$$\varepsilon_\alpha = \frac{a_\alpha - a_{\alpha 0}}{a_\alpha} \qquad (\alpha = 1,2,3) \tag{22}$$

$$\varepsilon_\alpha = a_\alpha - a_{\alpha 0} \qquad (\alpha = 4,5,6) \tag{23}$$

where $a_{\alpha 0}$, i.e. a_0 above, is the initial unstressed lattice constant, a_α is the instantaneous stressed lattice parameter. Since only a hydrostatic stress is applied, both the shear strains ε_α and shear stresses σ_α $(\alpha = 4,5,6)$ equal to zero.

The normal stress σ_α acting on a face of the unit cell is defined by the first order derivative of internal energy E_i with respect to the normal strain ε_α

$$\sigma_\alpha = \frac{1}{\Omega}\frac{\partial E_i}{\partial \varepsilon_\alpha}\bigg|_{\{a_\alpha\}} \qquad (\alpha = 1,2,3) \tag{24}$$

The elastic parameters $C_{\alpha\beta}$ which can be expressed in terms of the second derivatives of the internal energy with respect to the lattice strains ε_α.

$$C_{\alpha\beta} = \frac{1}{\Omega}\frac{\partial^2 E_i}{\partial \varepsilon_\alpha \partial \varepsilon_\beta}\bigg|_{\{a_\alpha\}} \qquad (\alpha,\beta = 1,2,3,4,5,6) \tag{25}$$

Based on the crystal symmetry of the crystal and using Eqs. (1)-(3) and (22)-(25), we can get:

$$\sigma_\alpha = \frac{1}{\Omega}\left[F'(\rho)\sum_j f'(r_j)\frac{r_{j\alpha}^2}{r_j} + \frac{1}{2}\sum_j \phi'(r_j)\frac{r_{j\alpha}^2}{r_j} + 2M'(P)\sum_j f(r_j)f'(r_j)\frac{r_{j\alpha}^2}{r_j}\right]\left(\frac{a_0}{a_\alpha}\right) \tag{26}$$

$$C_{\alpha\beta} = \frac{1}{\Omega}\Bigg\{F''(\rho)\left[\sum_j \frac{r_{j\alpha}r_{j\beta}}{r_j}f'(r_j)\right]^2 + F'(\rho)\sum_j\left(\frac{r_{j\alpha}r_{j\beta}}{r_j}\right)^2\left[f''(r_j) - \frac{f'(r_j)}{r_j}\right] + F'(\rho)\sum_j \delta_{\alpha\beta}\frac{r_{j\alpha}r_{j\beta}}{r_j}f'(r_j)$$

$$+\frac{1}{2}\sum_j\left(\frac{r_{j\alpha}r_{j\beta}}{r_j}\right)^2\left[\phi''(r_j) - \frac{\phi'(r_j)}{r_j}\right] + \frac{1}{2}\sum_j \delta_{\alpha\beta}\frac{r_{j\alpha}r_{j\beta}}{r_j}\phi'(r_j) + 4M''(P)\left[\sum_j f(r_j)f'(r_j)\frac{r_{j\alpha}r_{j\beta}}{r_j}\right]^2$$

$$+2M'(P)\sum_j\left(\frac{r_{j\alpha}r_{j\beta}}{r_j}\right)\left[f'^2(r_j) + f(r_j)f''(r_j) - \frac{f(r_j)f'(r_j)}{r_j}\right]$$

$$+2M'(P)\sum_j \delta_{\alpha\beta}\left(\frac{r_{j\alpha}r_{j\beta}}{r_j}\right)f(r_j)f'(r_j)\Bigg\}\left(\frac{a_0^2}{a_\alpha a_\beta}\right) \tag{27}$$

If $\alpha = \beta$, $\delta_{\alpha\beta} = 1$, or else $\delta_{\alpha\beta} = 0$.

where r_j, i.e. r_{ij} above, is the separation distance of atom *j* from atom *i*, the subscript *i* is neglected here since the site i is selected as the origin of the coordinate system.

Under hydrostatic loading, the applied pressure P equals to the negative normal stress on each plane, viz. $P = -\sigma_1$ $(= -\sigma_2 = -\sigma_3)$. Three principal edges of the cubic lattice cell a_1, a_2 and a_3 remain equal to each other throughout the hydrostatic loading and their included angles a_4, a_5 and a_6 will retain their initial values of $\pi/2$ (at least until failure occurs) due to no shear stresses.

For a cubic system under hydrostatic loading, the stability criteria are expressed as follows

$$\kappa = \frac{1}{3}(C_{11} + 2C_{12} + 2P) > 0 \tag{28}$$

$$\mu = \frac{1}{2}(C_{11} - C_{12} - P) > 0 \tag{29}$$

$$\mu' = C_{44} - P > 0 \tag{30}$$

where κ is bulk modulus, μ and μ' are the shear moduli, P is the applied pressure at current strain. The above stability criteria are presented by Born and then modified by Milstein. The theoretical strength is the value of the stress at which anyone of the above three conditions is not satisfied.

3. Results and Discussions

The variation of the internal energy per atom E_i, the normal stress σ_1, the stability criteria as a function of the principal stretch λ ($= \lambda_1 = \lambda_2 = \lambda_3 = a / a_0$) are shown in Figure 1-3. Only the stability criteria of Fe are given in Figure 3 since the similar curves are obtained for V, Nb and Ta.

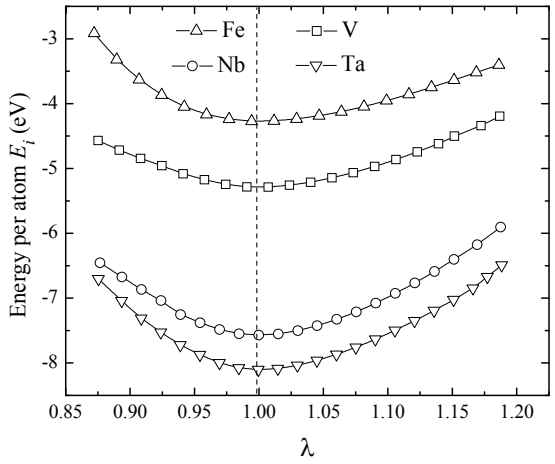

Figure 1. Energy per atom as a function of $\tilde{\lambda}$

From Figure 1, it can be seen that, for BCC crystal Fe, V, Nb, and Ta under hydrostatic loading, whether compressive or tensile loading from initial state, the internal energy per atom E_i are all increased. Such behavior is due to the work which is done by applied stresses and the initial stress-free state corresponds to the minimum energy. The result of the internal energy per atom E_i for Fe is similar to that of the Ab initio calculations.

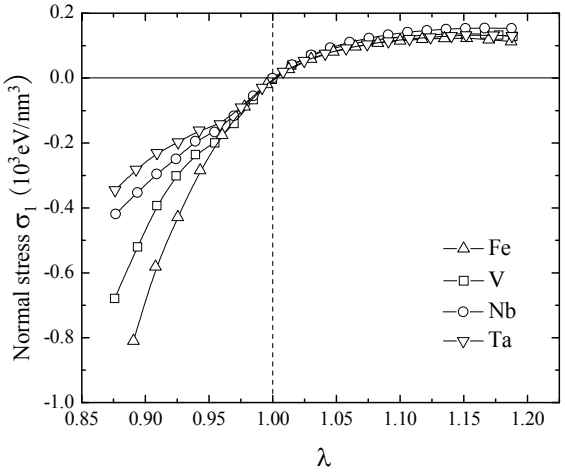

Figure 2. Normal stress as a function of $\tilde{\lambda}$

From Figure 2, we can see that, with decreasing the lattice stretch λ from initial stress-free state, the compressive stress σ_1 increases monotonously and quickly for Fe. However, the compressive stress σ_1 increases quickly at first and then slightly for V, Nb and Ta. The increased sequence of the compressive stress with decreasing λ is for Fe, V, Nb and Ta. While with increasing the lattice stretch λ from initial state, the tensile stress increases till the maximum tensile stress $\sigma_{\max}$ is reached and then decreases slightly. The calculated maximum tensile stresses $\sigma_{\max}$ are 123.57, 131.74, 154.45 and 137.85ev/nm^3, and the corresponding lattice stretch $\lambda_{\max}$ are 1.1527, 1.1617, 1.1661 and 1.1545 for Fe, V, Nb, Ta, respectively (listed in Table 3 for convenient). The maximum tensile stress $\sigma_{\max}=123.57\text{eV/nm}^3$ and the corresponding lattice stretch $\lambda_{\max}=1.1527$ of Fe approach to the results of $26.7\,\text{GPa}$ and the corresponding $\lambda_{\max}=1.15$ calculated by Ab initio with generalized gradient approximation (GGA).

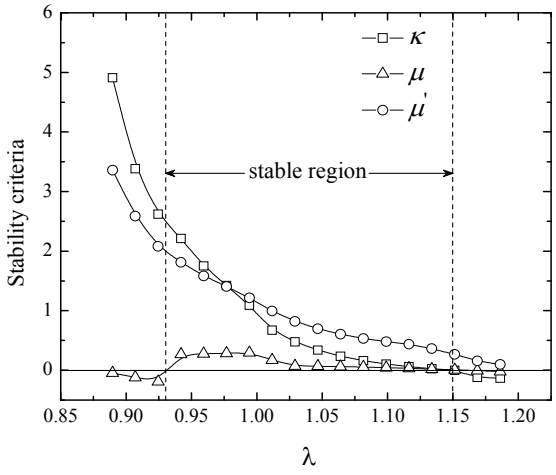

Figure 3. The stable criteria as a function of λ for Fe

From Figure 3, it can be seen that, the bulk modulus κ and the shear modulus μ' of Fe decrease with increasing λ. At $\lambda=1.1495$, the shear modulus κ passing through zero and the condition $\kappa>0$ is violated. The shear modulus μ decreases firstly and then increases passing through zero at $\lambda=0.9269$ with increasing λ. Then the shear modulus μ increases continually till to the maximum and then decreases passing through zero at $\lambda=1.1683$. So the stable region of Fe is 0.9269~1.1495 in the lattice stretch λ. The similar curves are obtained for V, Nb and Ta and the stable regions are determined to be 0.9270~1.1545, 0.9268~1.1449 and 0.9268~1.1427 in the lattice stretch λ, respectively. The corresponding compressive and tensile theoretical strengths are 408.89 and 123.54, 186.96 and 131.43, 259.07 and 152.53, 283.92 and 137.04eV/nm^3 for Fe, V, Nb, Ta respectively (listed also in Table 3 for convenient).

It is interesting to note that from Table 3, for each of the four crystals, the tensile strength is slightly lower than its maximum tensile stress. Second, the compressive strength is higher than tensile strength especially for Fe. Third, the stable regions are almost equal with respect to the lattice stretch λ, especially in compressive region.

Table 2. The calculated parameters for Fe, V, Nb and Ta, n and f_e are dimensionless, F_0, α and k_i are in eV

Metals	n	α	F_0	f_e	k_0	k_1	k_2	k_3
Fe	0.2778	0.0173	2.4900	0.3937	-0.3495	-0.2983	0.2765	0.1020
V	0.4782	0.1163	3.2100	0.4153	0.4452	-1.3959	0.6278	0.0203
Nb	0.6186	0.1328	4.8200	0.4539	0.7943	-2.0786	0.8912	0.0003
Ta	0.3605	0.1742	5.1500	0.4718	0.0071	-1.1755	0.6406	0.0939

Table 3. The maximum tensile stress σ_{max} and the corresponding lattice stretch λ_{max}, the stable region represented in lattice stretch λ and the compressive and tensile strengths for BCC metals Fe, V, Nb and Ta

Metals	σ_{max} (eV/nm^3)	λ_{max}	Stable Region	Theoretical Strength (eV/nm^3)	
				compressive	tensile
Fe	123.57	1.1527	0.9269~1.1495	408.89	123.54
V	131.74	1.1617	0.9270~1.1545	186.96	131.43
Nb	154.45	1.1661	0.9268~1.1449	259.07	152.53
Ta	137.85	1.1545	0.9268~1.1427	283.92	137.04

4. Conclusions

The structural stability and theoretical strength of BCC crystals Fe, V, Nb and Ta under hydrostatic loading have been investigated by combining the MAEAM with Milstein modified Born stability criteria. The conclusions are summarized as follows:

(1) For all four BCC crystals under hydrostatic loading, as expected whether compressive or tensile loading from initial state, the internal energy per atom E_i are all increased.

(2) The failures occur while the condition $\mu>0$ is violated in compressive region and $\kappa>0$ is violated in tensile region.

(3) The stable regions are almost equal with respect to the lattice stretch λ, especially in compressive region.

(4) For each of the four crystals, the tensile strength is slightly lower than the maximum tensile stress, however, the compressive strength is higher than tensile strength especially for Fe.

References

Černý, M., Pokluda, J., Šob, M., Friák, M., & Šandera, P. (2003). Ab initio calculations of elastic and magnetic properties of Fe, Co, Ni, and Cr crystals under isotropic deformation. *Phys. Rev. B*, 035116.

Clatterbuck, D. M., Chrzan, D. C., & Morris Jr, J. W. (2003). The influence of triaxial stress on the ideal tensile strength of iron. *Scripta Mate*r, 1007. http://dx.doi.org/10.1016/S1359-6462(03)00490-1

de la Fuente, O. R., Zimmerman, J. A., González, M. A., de la Figuera, J., & Hamilton, J. C. (2002). Dislocation Emission around Nanoindentations on a (001) fcc Metal Surface Studied by Scanning Tunneling Microscopy and Atomistic Simulations. *Phys. Rev. Lett.*, 88. http://link.aps.org/doi/10.1103/PhysRevLett.88.036101

Hu, W. Y., Shu, X. L., & Zhang, B. W. (2002). Point-defect properties in body-centered cubic transition metals with analytic EAM interatomic potentials. *Comput. Mater. Sci*., 175. http://dx.doi.org/10.1016/S0927-0256(01)00238-5

Kanchana, V., Vaitheeswaran, G., & Rajagopalan, M. (2003). Structural phase stability of CaF_2 and SrF_2 under pressure. *Physica B*, 283. http://dx.doi.org/10.1016/S0921-4526(02)01851-3

Kelly, A. (1966). *Strong Solids.*

Kelly, A., & Macmillan, N. H. (1986). *Strong Solids*.

Li, H. T., Zhang, J. M., & Xu, K. W. (2008). Stability of BCC transition metals under hydrostatic loading. *Mater. Sci. Eng. A*, 627. http://dx.doi.org/10.1016/j.msea.2007.08.024

Milstein, F., & Chantasiriwan, S. (1998). Theoretical study of the response of 12 cubic metals to uniaxial loading. *Phys. Rev. B*, 6006. http://dx.doi.org/10.1103/PhysRevB.58.6006

Milstein, F., & Huang, K. (1978). Theory of the response of an fcc crystal to [110] uniaxial loading. *Phys. Rev. B*, 2529. http://dx.doi.org/10.1103/PhysRevB.18.2529

Qi, L., Zhang, H. F., & Hu, Z. Q. (2004). *Intermetallics,* p1191. Molecular dynamic simulation of glass formation in binary liquid metal: Cu–Ag using EAM. http://dx.doi.org/10.1016/j.intermet.2004.04.003

Saib, S., & Bouarissa, N. (2007). Structural phase transformations of GaN and InN under high pressure. *Physica B*, 377. http://dx.doi.org/10.1016/j.physb.2006.04.023

Zhang, J. M., Li, H. T., & Xu, K. W. (2007). The stability of FCC crystal Ni under uniaxial loading. *Solid State*

Commun., 535. http://dx.doi.org/10.1016/j.ssc.2007.01.001

Zhang, J. M., Wang, J. Z., Xu, K. W., & Ji, Vincent. (2008b). *Cryst. Res. Technol*., 828. Retrieved from http://onlinelibrary.wiley.com/journal/10.1002/(ISSN)1521-4079/earlyview

Zhang, J. M., Yang, Y, Xu, K. W., & Ji, Vincent. (2008a). *Can. J. Phys*., 935. Retrieved from http://academic.research.microsoft.com/Search?query=J%20M%20Zhang